Earth, Planets and Space
a SpringerOpen Journal

FULL PAPER Open Access

The propagation of ULF waves from the Earth's foreshock region to ground: the case study of 15 February 2009

Mauro Regi*, Marcello De Lauretis, Patrizia Francia and Umberto Villante

Abstract

A long-duration upstream ultralow frequency (ULF) wave event was detected on 15 February 2009 by Cluster satellites, close to the bow shock nose. A clear wave activity was identified when the interplanetary magnetic field orientation was favorable to the local generation. We examined the wave properties in both the solar wind and the spacecraft frame during a selected time interval and found that foreshock waves were essentially Alfven waves propagating at a small angle with respect to the interplanetary magnetic field. A comparison of Cluster observations with those on the ground, in the polar cap and at low-latitude stations, confirms the results of previous studies, indicating that upstream waves can reach different ground regions along different paths.

Keywords: Upstream ULF waves; Doppler shift; Geomagnetic pulsations

Background

The propagation to the ground of mid-frequency (10 to 100 mHz) ultralow frequency (ULF) waves generated upstream the Earth's bow shock is a much debated subject. Such waves are the result of a wave-particle interaction between already-existing waves and solar wind (SW) protons reflected off the bow shock, and mostly occur in the region of quasi-parallel bow shock, i.e., where the interplanetary magnetic field (IMF) makes a small angle θ_{nB} (<45°) with the shock normal (Regi et al. 2014 and references therein). They propagate sunwards at speeds close to the local Alfven speed in the SW rest frame but are convected by the faster SW in the opposite direction. Russell et al. (1971) discussed that the foreshock waves are left-hand polarized in the spacecraft frame, while they are intrinsically right-hand polarized, resulting from the reversal of phase speed direction; in addition, the wave frequency in the spacecraft frame is modified by the Doppler shift: $\omega_{sc} = \omega_r + \boldsymbol{k}\cdot\boldsymbol{V}_{SW}$, where ω_{sc}, ω_r, $\boldsymbol{k}$, and $\boldsymbol{V}_{sw}$ represent the angular frequency in the spacecraft frame and in the SW frame, the wave number vector, and the SW flow velocity, respectively (Narita et al. 2004).

The waves propagate through the bow shock and magnetosheath towards the magnetopause and can be transmitted into the magnetosphere and reach the ground, without significant changes in their spectrum (Krauss-Varban and Omidi 1991).

Different propagation paths through the magnetosphere have been suggested to explain their occurrence at different latitudes. From low to high latitudes, the mostly daytime occurrence of fluctuations is explained in terms of waves generated upstream of the bow shock nose and transmitted through the subsolar region into the magnetosphere as compressional waves (Russell et al. 1983); the inward propagating waves can couple, due to magnetospheric inhomogeneities, to field-guided Alfven modes on closed field lines and reach the ground, driving resonant oscillations at latitudes where the incoming wave frequency matches the local field line eigenfrequency or its harmonics (Chen and Hasegawa 1974; Yumoto 1985; Menk et al. 2000; Howard and Menk 2005).

In the polar cap, where the local field lines are stretched into the magnetotail, the results of Francia et al. (2012) and Regi et al. (2013) indicate that a different transmission and propagation path can be invoked, as already suggested by Chugunova et al. (2004, 2006) and Engebretson et al. (2006): the waves, convected along the flanks of the magnetopause by the SW, penetrate through the plasma

* Correspondence: mauro.regi@aquila.infn.it
Dipartimento di Scienze Fisiche e Chimiche, Università degli Studi dell'Aquila, L'Aquila 67100, Italy

mantle and magnetotail lobes, where they can couple to traveling field-guided Alfven waves along the outermost open field lines and propagate to the polar cap. The mechanism of the mode conversion on open field lines has not been reliably identified yet (Pilipenko et al. 2008).

In the present study, we analyzed a long-duration ULF wave event detected on 15 February 2009 by Cluster satellites, located in the SW in front of the bow shock nose, examining the wave properties in both the SW and spacecraft frame. The results of a comparison of the Cluster observations with those on the ground appear consistent with the upstream waves propagating through the magnetosphere up to the polar cap and to low-mid latitudes along different paths.

Methods

For monitoring the upstream region, we used the measurements from the four Cluster satellites, in particular, the magnetic field data from the triaxial fluxgate magnetometer (FGM) (Balogh et al. 2001) and the SW data from Cluster Ion Spectrometer (CIS) (Rème et al. 2001); both measurements are in the Geocentric Solar Ecliptic (GSE) coordinate system and have a time resolution of 4 s. On the ground, we analyzed the search-coil magnetometer data at Dome C (DMC) and Terra Nova Bay (TNB), in Antarctica, and the fluxgate magnetometer data from the South European GeoMagnetic Array (SEGMA; http://sole-terra.aquila.infn.it/staz_segma.asp) stations Nagycenk (NCK; Hungary) and Castello Tesino (CST; Italy) (see Table 1 for details).

For the signal identification, we adopted a technique similar to that described by De Lauretis et al. (2010) to separate the upstream-related band-limited enhancement and the power law background in the spectral domain. In particular, we analyzed the frequency-time dependence of the signal-to-noise ratio R over a 20-min interval (nominal frequency resolution ~0.83 mHz), the beginning of each interval being shifted by 1 min with respect to the preceding (time resolution of 1 min). The resulting spectra were smoothed over nine frequency bands, using a triangular window (final frequency resolution is ~4.16 mHz). Because fluxgate and search-coil magnetometer have a different frequency response, we differentiated the fluxgate time series before computing the spectra in order to reduce the spectral slope. After the smoothing procedure, the fluxgate spectra were corrected for the frequency response of the differential filter, while the search-coil spectra were corrected for their transfer function in order to convert the power spectral densities from V^2/Hz to nT^2/Hz (see, for example, De Lauretis et al. 2010).

The R peak frequency was compared with the predicted wave frequency in the spacecraft frame obtained from the Takahashi et al. (1984) original formula, i.e., releasing the assumption of waves generated at the shock nose (Francia et al. 2012):

$$f(\mathrm{mHz}) = 7.6B\cos\theta_{xB}\cos\theta_{nB}/\cos\theta_{xn}, \quad (1)$$

where θ_{xB} is the cone angle (i.e., the angle between the sunward direction $\boldsymbol{x}$ and the local IMF $\boldsymbol{B}$), θ_{nB} is the angle between the IMF and the bow shock normal, and θ_{xn} is the angle between the bow shock normal and the $\boldsymbol{x}$ direction. For each interval, B was computed from the 20-min running averages of all the IMF components, i.e., $<B> = (<B_x>^2 + <B_y>^2 + <B_z>^2)^{1/2}$. The cone angle was computed as $\theta_{xB} = \cos^{-1}(|<B_x>|/<B>)$; the angles θ_{xn} and θ_{nB} were computed considering the bow shock normal, where the IMF line at the spacecraft position encounters the bow shock, as obtained from the Kobel and Flückiger (1994) bow shock model. Such model allows us also to estimate the magnetic field intensity and direction in the magnetosheath, on the basis of the observed IMF and for a given position of the stand-off distance of the magnetopause (R_{mp}) and bow shock (R_{bs}). The parameters $R_{\mathrm{mp}} = 10\ R_{\mathrm{E}}$ and $R_{\mathrm{bs}} = 15.6\ R_{\mathrm{E}}$ (1 R_{E} = 6,380 km) were evaluated using the Peredo et al. (1995) bow shock model and the Shue et al. (1997) magnetopause model.

We also investigated the upstream wave propagation in the foreshock, using the Wave Telescope technique (Glassmeier et al. 2001); the analysis was restricted to the time interval when the satellite configuration was characterized by a quality index $Q > 2$ ($Q = 3$ corresponds to an ideal tetrahedron structure; Glassmeier et al. 2001), allowing us to better identify the wave vector $\boldsymbol{k}$. In particular, we evaluated the $\boldsymbol{k}$ vector at the different frequencies and analyzed the dispersion relation to obtain the phase speed ($\boldsymbol{V}_{\mathrm{sc}}$) in the spacecraft reference

Table 1 Geographic and geomagnetic coordinates, LT, and MLT for the ground geomagnetic stations

IAGA code	Geographic coordinates	Corrected geomagnetic coordinates (IGRF05)	Local time (LT)	Magnetic local time (MLT)
DMC	75.10 S, 123.38 E	88.89 S, 54.58 E	LT ~ UT + 8	MLT ~ UT – 1
TNB	74.69 S, 164.12 E	80.01 S, 306.94 E	LT ~ UT + 11	MLT ~ UT – 8
NCK	47.63 N, 16.72 E	42.79 N, 91.41 E	LT ~ UT + 1.1	MLT ~ UT + 1.8
CST	46.05 N, 11.65 E	40.84 N, 86.63 E	LT ~ UT + 0.8	MLT ~ UT + 1.5

frame. Then, $\boldsymbol{V}_{sc}$ was converted into the SW rest frame $\boldsymbol{V}_r$, removing the background flow velocity $\boldsymbol{V}_{SW}$

$$\boldsymbol{V}_r = \boldsymbol{V}_{sc} - \boldsymbol{V}_{SW}, \tag{2}$$

and the wave frequency was corrected for the Doppler shift using the relation

$$\omega_r = \omega_{sc} - \boldsymbol{k}\cdot\boldsymbol{V}_{SW} \tag{3}$$

Results and discussion

Upstream waves in the foreshock region

Figure 1 shows the Cluster 1 position in the GSE *X-Y* and *X-Z* planes together with the bow shock and magnetopause profile from the Kobel and Flückiger model (upper panels), the SW speed V_{SW}, particle density n, anisotropy temperature index $T_\parallel/T_\perp$ and IMF components (lower panels). We show the original IMF data (at 4 s), while the SW data are 20-min running averages with a step of 1 min. The anisotropy temperature index is useful to identify the magnetosheath with respect the upstream region: indeed, on the basis of a case study (Francia et al. 2013) and a statistical study (Regi et al. 2014), the transition in the magnetosheath can be associated to a value of the temperature ratio lower than ~2 (dashed horizontal line in Figure 1). During 00 to 1640 UT, the temperature ratio was higher than 2, indicating that the satellite was in the upstream region (in agreement with the Kobel and Flückiger bow shock model), then it decreased (the vertical red dashed lines indicate the transition region), reaching values lower than 2 around

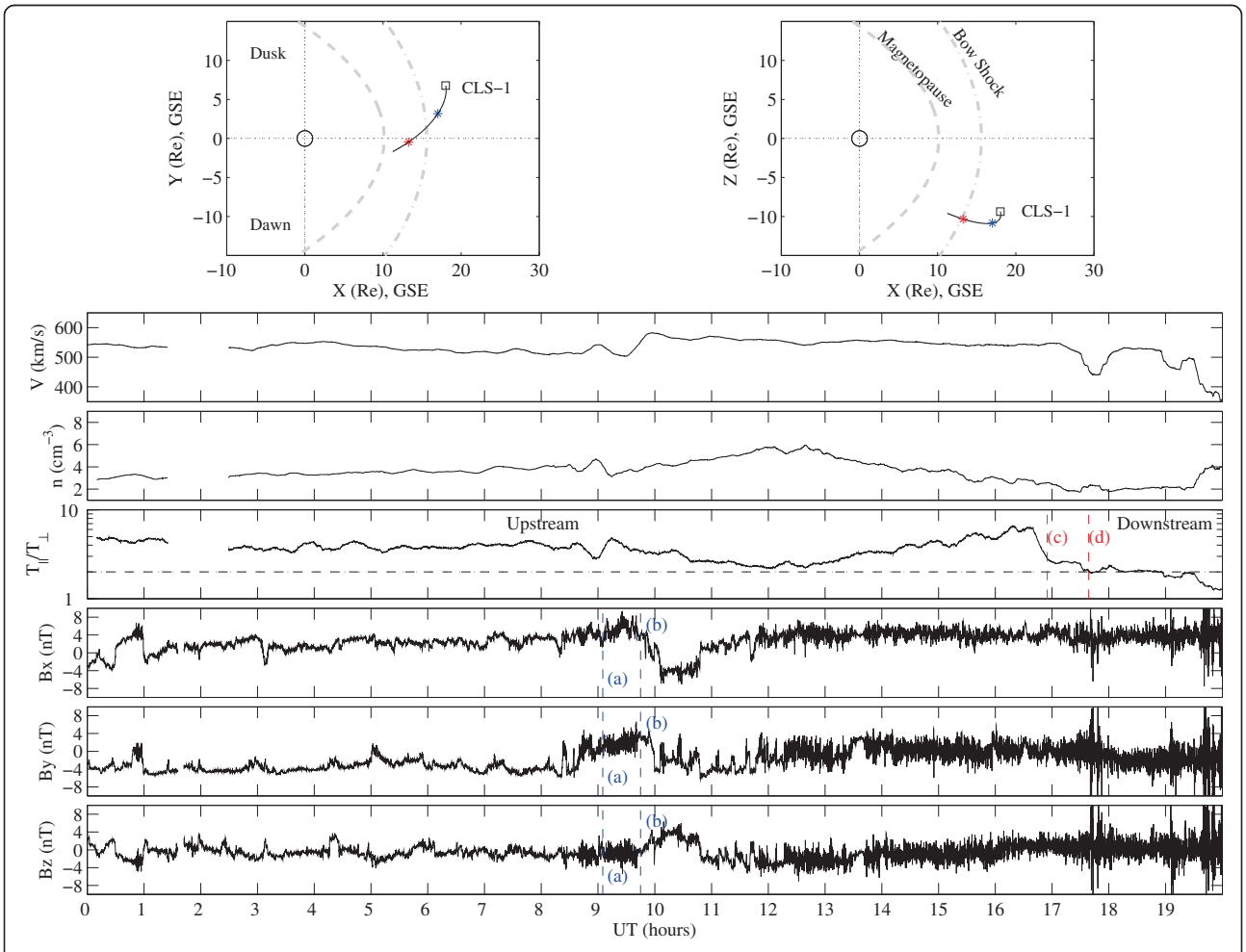

Figure 1 Cluster 1 position in the GSE *X-Y* and *X-Z* planes and IMF and SW data. Upper panels: the Cluster 1 satellite orbit on 15 February 2009 projected in the *X-Y* (left) and *Y-Z* (right) plane in the GSE coordinate system, together with the bow shock and magnetopause profiles (dashed gray lines). Lower panels from top to bottom: the 20-min running averages of SW speed V_{SW}, plasma number density n, and anisotropy temperature ratio $T_\parallel/T_\perp$, and the 4-s IMF components B_x, B_y, and B_z. Vertical red dashed lines (c and d labels) mark the transition region from upstream to downstream conditions (in the upper panels, the red asterisk indicates the Cluster position), while the vertical blue dashed lines (a and b labels) delimit the time interval analyzed by the Wave Telescope technique (in the upper panels, the blue asterisk indicates the Cluster position).

1740 UT (revealing a bow shock oscillation which, on the basis of the satellite position at ~1725 UT and ~1800 UT, we estimated as wide as ~2,700 km) and after 1900 UT. Consistently, V_{SW} was almost stable during 00 to 1640 UT with an average value of ~540 km/s, while it decreased to ~390 km/s at ~1740 UT and ~1910 UT.

In the upstream region, the IMF conditions were quite stable up to ~0840 UT, when clear fluctuations were observed in all components. Between ~0950 UT and ~12 UT, the IMF fluctuations disappeared; then, they were newly observed for the rest of the time.

In Figure 2, we show the angles θ_{xB} and θ_{nB} (upper panel), the frequency-time dependence of R for the three IMF components (middle panels) together with the upstream wave frequency predicted by (1), and the Q index (lower panel). The angle θ_{nB} is not shown when the satellite was not connected to the bow shock through the IMF line, or IMF data were not available. Below the upper panel, we evidenced, on the basis of the θ_{nB} value, the favorable ($\theta_{nB} < 45°$, red) and unfavorable ($\theta_{nB} > 45°$, yellow) conditions for the upstream wave generation. High signal-to-noise ratio, approximately at the predicted frequency, was observed only during the time intervals ~0830 to 1030 and 1200 to 1730 UT, in correspondence to the favorable conditions. These signals emerged more clearly in the B_y and B_z components.

Figure 3 shows the position of Cluster with respect to the bow shock sector (shown in thin red) where upstream waves could be generated (i.e., where $\theta_{nB} < 45°$), in correspondence to the different UTs indicated by the dotted lines in the middle panels of Figure 2. At ~0630 UT and ~1110 UT, the satellites were not magnetically connected with the foreshock region; these conditions lead to the absence of ULF signals at Cluster. Instead, a favorable IMF orientation was observed at ~0925 UT and ~1300 UT, when waves were effectively detected by Cluster.

To examine the wave properties, we selected the 0905- to 0945-UT interval (indicated by the vertical blue dashed lines in Figures 1 and 2) corresponding to a quality index $Q > 2$ and to a quite stable average IMF, $\boldsymbol{B} = (5.2 \pm 1.0, 1.9 \pm 0.5, -0.8 \pm 0.5$ nT), thus suitable to be studied using the Wave Telescope technique. The wave number resolution for the Cluster configuration during this interval is $\delta k \sim 10^{-5}$ rad/km. Figure 4a shows the time series of the IMF components in the GSE coordinate system; the fluctuations were more pronounced in the B_y and B_z components. We first computed the power spectra applying Welch's method, using a running window of 512 s (128 samples at 4 s), with a step size of 128 s (32 samples). The spectrum of each component (Figure 4b) shows a broad band enhancement in the 20- to 50-mHz frequency range.

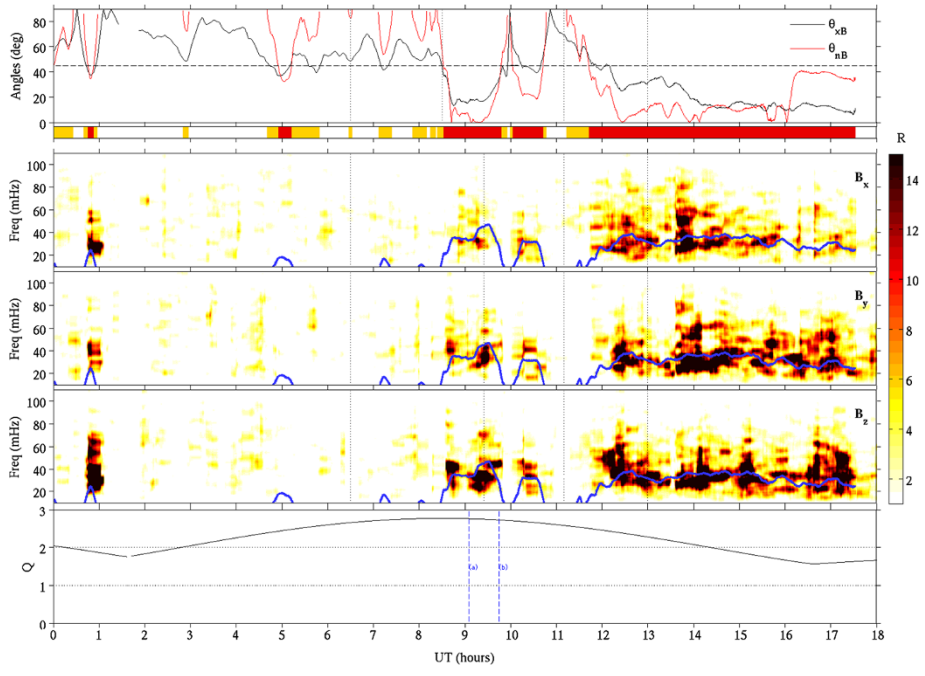

Figure 2 The angles θ_{xB} and θ_{nB} and the frequency-time dependence of R for the IMF components. The cone angle θ_{xB} (black) and the angle θ_{nB} (red) at Cluster 1 position during the time interval 00 to 18 UT on 15 February 2009 (upper panel); favorable (red) and unfavorable (yellow) conditions for upstream wave occurrence are evidenced in the thick bar below. The dynamic signal-to-noise ratio R for B_x, B_y, and B_z in a color scale (middle panels), together with the predicted upstream wave frequencies (blue line). The quality index Q of Cluster satellites (lower panel); the vertical blue dashed lines (a and b labels) indicate the 0905- to 0945-UT interval analyzed through the Wave Telescope technique.

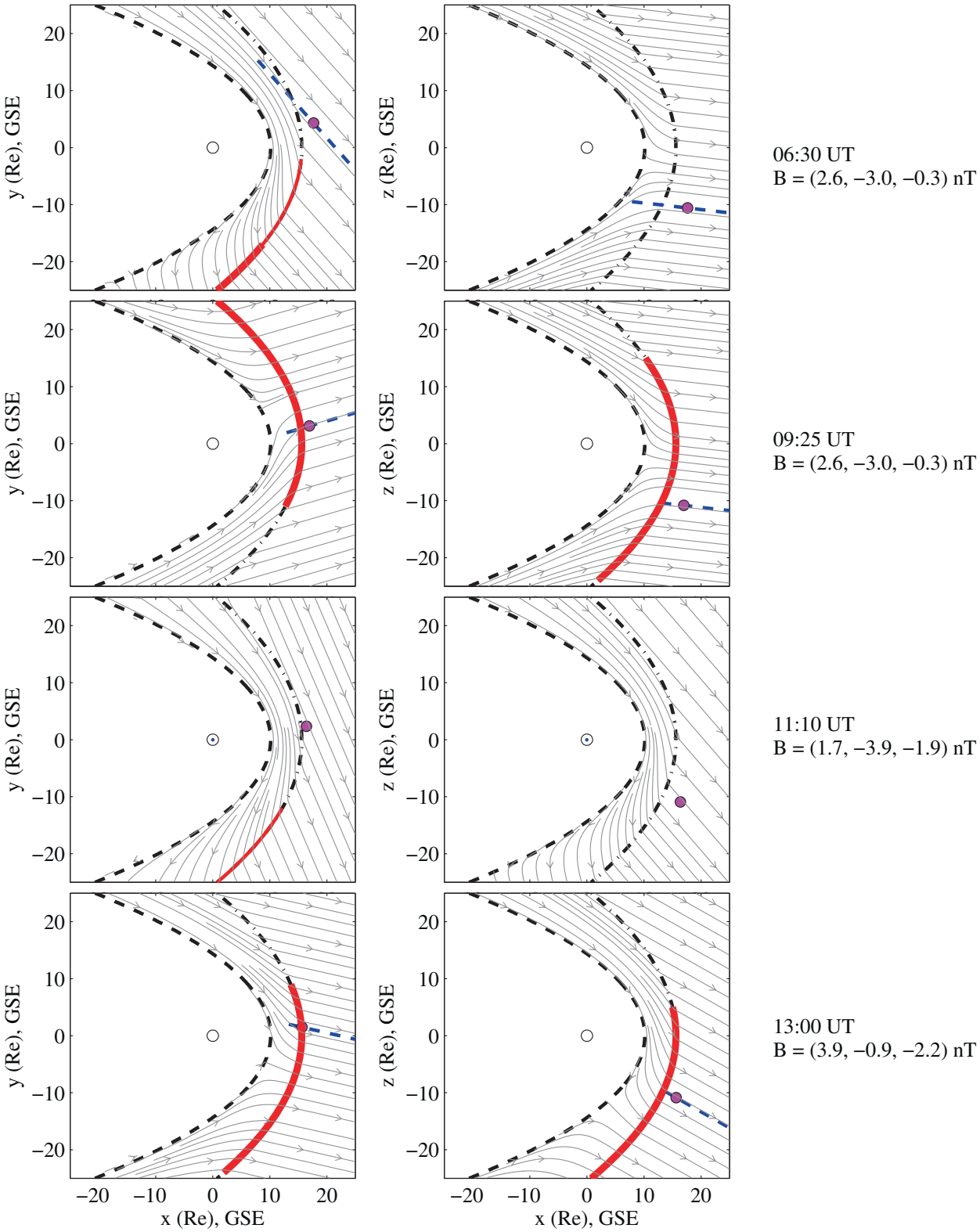

Figure 3 The Cluster 1 position at times of interest. The Cluster 1 position (magenta filled circle) with respect to the magnetopause and bow shock profile from the Kobel and Flückiger model (dashed black lines) in the GSE *X-Y* (left) and *X-Z* (right) planes, together with the IMF and magnetosheath lines at different times. The red portion on the bow shock indicates the wave generation region, while the thick red portion refers to the region where waves observed on the ground were generated. The blue line represents the IMF line connecting the spacecraft to the bow shock.

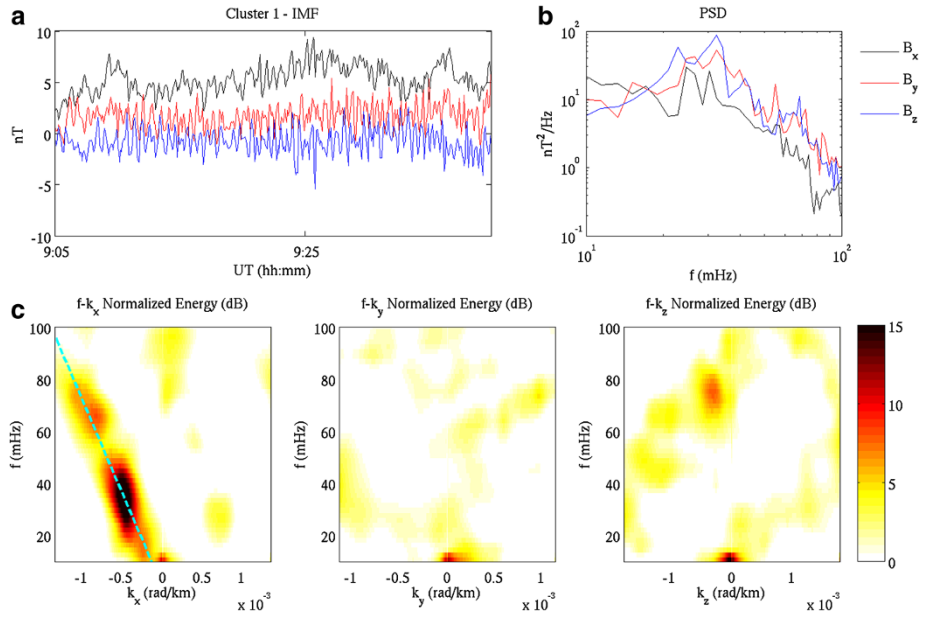

Figure 4 The Wave Telescope analysis in the time interval 0905 to 0945 UT. (a) The time series of IMF components on Cluster 1 satellite. **(b)** The related power spectral densities. **(c)** The normalized energy density (color scale) as a function of frequency f and wave number vector k. The dashed line indicates the linear relationship between frequency and wave number for the energy maximum in $k_x < 0$ domain.

Then, applying the Wave Telescope analysis, we obtained the dispersion diagrams (f-k) in the spacecraft reference frame (Figure 4c), where $f = \omega / 2\pi$ is the wave frequency. The energy in the f-k space was normalized to a background value estimated through an iterative and convergent procedure (Vellante et al. 1989); at any step, the average energy spectrum $E(f)$ over all k was recomputed, removing all the spectra with enhancements at any frequency greater than $E(f) + 3\sigma$. The energy associated to k_y and k_z was found negligible at all frequencies with respect to the energy associated to k_x, suggesting a wave propagation approximately along the Earth-Sun direction. The waves propagated earthward, as shown by the energy maximum at $k_x < 0$ for the frequency range of interest. Considering that the average IMF, $\boldsymbol{B} = (5.2, 1.9, -0.8$ nT), was at an angle ~160° with the earthward direction, the wave propagation was approximately antiparallel to the field. High energy values are distributed along a straight line, whose slope is proportional to the wave phase velocity in the spacecraft frame:

$$V_{sc} = 2\pi f / k \tag{4}$$

We estimated the phase velocity $V_{sc} = -439 \pm 15$ km/s earthward in the $\boldsymbol{x}$ direction; since the average SW speed was essentially in the same direction, $\boldsymbol{V}_{SW} = (-515, 14, 14) \pm 20$ km/s, using relation (2), we found that the wave phase velocity in the SW rest frame was $V_r = 76 \pm 25$ km/s in the sunward direction. During this period, the average IMF strength and plasma number density were $B = 5.6 \pm 1.4$ nT and $n = 3.4 \pm 0.8$ cm^{-3}, respectively, and hence, the Alfvèn velocity was $V_A = B/(\mu_0 \rho)^{1/2} = 66 \pm 20$ km/s, well consistent with the estimated V_r. Moreover, the Doppler shift $\Delta\omega = k_x V_{SW}$ at each frequency as obtained by inverting relation (4), $k_x = 2\pi f / V_{sc}$, was

$$\Delta f = \Delta\omega / 2\pi = (V_{SW} / V_{sc}) f \tag{5}$$

Using this relation, with $V_{SW}/V_{sc} \sim 1.17$, we estimated the wave frequency in the SW rest frame as

$$f_r = (1 - V_{SW}/V_{sc}) f \sim -0.17 f \tag{6}$$

The negative wave frequency f_r is related to the reversal of the phase speed direction in the SW frame (see Narita et al. 2004). Considering the predominant peak at f_{sc} ~32 mHz in the power spectra of Figure 4b (B_y and B_z components), the corresponding wave frequency in the SW rest frame is $f_r \sim -5$ mHz.

Ground observations of geomagnetic pulsations

In Figure 5, the frequency-time dependence of R for the horizontal H and D components at the ground stations is shown together with the predicted frequency at the Cluster position. Since the ULF signals observed at ground could propagate from a not *a priori* identified region, we looked for a possible source region on the basis of formula (1), in which the wave frequency depends on θ_{nB}; for each $\boldsymbol{B}$, we varied θ_{nB} between 0° and 45° (moving then along the bow shock) to evaluate the highest (f_h) and lowest frequency (f_l) in correspondence

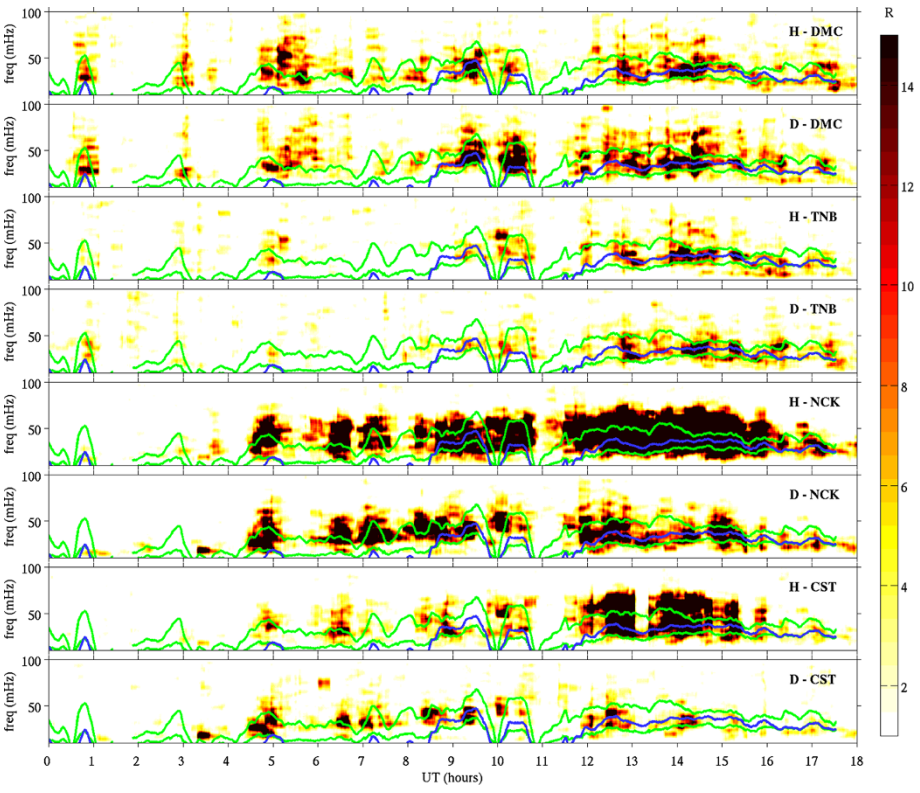

Figure 5 The dynamic *R* at ground stations. The dynamic signal-to-noise ratio *R* (color scale) at ground stations on 15 February 2009, in the *H* and *D* horizontal components of the geomagnetic field. In each row, the green lines indicate the highest (f_h) and lowest frequency (f_l) in correspondence to the boundaries of the favorable generation region, while the blue line shows the predicted frequency at the Cluster 1 satellite position.

to the boundaries of the favorable generation region (Regi et al. 2014). Also, these frequencies are plotted in the figure.

The ground spectra manifest a broad band activity. At DMC and TNB, in both components, the highest values of *R* follow closely the frequency predicted and observed at Cluster after 0830 UT; in addition, at DMC, high signals at frequencies close to f_h were observed also between 0500 and 0830 UT, when the wave activity was not detected at Cluster; such signals were less evident at TNB, whose field line was located in the local midnight sector (Table 1). Similarly, at NCK and CST in the *D* component, high *R* values were observed in correspondence to f_h from 0500 to 0830 UT; after 12 UT, the signals have frequencies similar to those observed simultaneously at high latitude and Cluster. In the *H* component, more clearly during 0430 to 1630 UT, the signals were affected by the resonance, whose frequency is typically around 60 mHz during low solar activity (Vellante et al. 2009), as during 2009.

From the values of the frequencies corresponding to high values of *R* on the ground around 0630, 0925, and 1300 UT, we inferred, using the Takahashi formula (1) and on the basis of the IMF direction, the possible source region, upstream of the bow shock portion indicated in thick red in Figure 3. Around 0925 and 1300 UT, the waves seem to propagate to the ground from an upstream region which includes the subsolar region where Cluster was located. On the other hand, around 0630 UT, the source region for the waves observed at CST, NCK, and DMC was restricted only in the early morning sector, consistently with the MLT of the stations.

Conclusions

On 15 February 2009, ULF waves were detected in the foreshock region during an interval of several hours. Cluster satellites, located approximately ahead the nose of the bow shock, observed a wave activity when the conditions were favorable to the local generation, due to the small angle θ_{nB} (<45°); the wave frequency follows approximately the frequency predicted by Takahashi et al. (1984).

A short time interval was analyzed, applying the Wave Telescope technique to investigate the properties of the propagating waves. Considering the energy peak at ~32 mHz in the spacecraft frame, we estimated an antisunward propagation approximately along the ambient field with predominantly transverse oscillations. A Doppler shift of ~37 mHz was evaluated, leading to a frequency

of approximately −5 mHz in the SW rest frame; the value of such frequency is of the same order of 0.1 Ω_c, where $\Omega_c \sim 80 \pm 20$ mHz is the estimated ion-cyclotron frequency, in agreement with Hoppe and Russell (1983) and Narita et al. (2004). The upstream waves propagated sunward in the SW frame, with a phase velocity close to the locally estimated Alfvèn velocity. These results indicate that the waves were essentially Alfven waves propagating at a small angle with respect to the IMF.

Our conclusions are consistent with the results of the statistical analysis by Narita et al. (2004), obtained applying the Wave Telescope technique to Cluster observations, which strongly support the existence of Alfven waves in the foreshock; they show that the distribution of the wave number magnitude k exhibits a peak between 0.5×10^{-3} and 1×10^{-3} km^{-1}, implying a propagation speed close to the Alfven velocity, and the propagation angle θ_{kB} is mostly at values smaller than 30° or greater than 160°, indicating parallel or antiparallel propagation to the magnetic field.

As matter of fact, both alfvenic and fast magnetosonic waves have been observed in the foreshock region (Hoppe and Russell 1983; Eastwood et al. 2002, 2003; Shevyrev et al. 2006). Interestingly, examining the ISEE observations during two events, Le and Russell (1992) found that upstream wave properties depend on their location in the foreshock: waves are weak, nearly transversal in the deep foreshock while become stronger and more compressional close to the bow shock.

On the ground, the ULF waves were observed from polar to low-latitude stations. The signal-to-noise ratio R showed a time-frequency evolution similar to that observed by the spacecraft between 0830 and 1730 UT, at low latitudes more clearly in the D component, not affected by resonant phenomena. In particular, during the 0905- to 0945-UT time interval, examined in detail at Cluster, the signals observed at CST and NCK were probably due to waves propagating radially from the generation region (as shown in Figure 3) and directly transmitted through the subsolar bow shock and into the magnetosphere as compressional waves up to the low latitude (Russell et al. 1983; Howard and Menk 2005). On the other hand, the occurrence of the same signals at the polar latitudes could be explained in terms of waves convected by the SW along the flanks of the magnetopause, penetrating into the magnetotail lobes and then propagating along the outer field lines to the ground, as already suggested by Chugunova et al. (2006), Engebretson et al. (2006), and Francia et al. (2012). In this regard, recently, Regi et al. (2013) provided experimental evidence of the suggested transmission path; on the basis of geomagnetic field measurements at DMC and simultaneous magnetospheric data from Cluster satellites in the southern lobe on field lines with footprints close to DMC (i.e., at an angular separation smaller than 15°), a clear correspondence between waves observed in the magnetotail and near the geomagnetic pole was found from a statistical point of view and in a case study. Both at low latitude and DMC (less evident at TNB), significant fluctuations were also observed between 0500 and 0830 UT; they did not find correspondence at Cluster. During this time period, in particular around 0630 UT, the values of the observed frequencies were consistent with waves generated and propagated from the region upstream of the early morning portion of the bow shock, so explaining the absence of signals at the satellite, which was located close to the shock nose. The much lower signals observed at TNB can be explained since, around the local magnetic midnight (~08 UT), the TNB field line was located more deeply in the magnetotail with respect to DMC; so, the waves at TNB were more attenuated (the relative position of the field lines are shown in De Lauretis et al. (2010)). Such behavior was already observed from the first ULF measurements at DMC, during 16 to 22 November 2003, as compared with the simultaneous TNB data (De Lauretis et al. 2005), when the wave power at TNB around local magnetic midnight was a factor ~3 to 5 smaller than at DMC, and from a statistical analysis of the MLT dependence of the ULF power at TNB and DMC during 2005 to 2007 (Francia et al. 2009).

Competing interests
The authors declare that they have no competing interests.

Authors' contributions
MR, MDL, PF, and UV participated in the design of the study and data analysis. All authors read and approved the final manuscript.

Received: 18 February 2014 Accepted: 8 May 2014
Published: 29 May 2014

References
Balogh A, Carr CM, Acuña MH, Dunlop MW, Beek TJ, Brown P, Fornaçon KH, Georgescu E, Glassmeier KH, Harris J, Musmann G, Oddy T, Schwingeschuh K (2001) The Cluster Magnetic Field Investigation: overview of in-flight performance and initial results. Ann Geophys 19:1207–1217

Chen L, Hasegawa A (1974) A theory of long-period magnetic pulsations: 1. Steady state excitation of field line resonance. J Geophys Res 79:1024–1037

Chugunova OM, Pilipenko VF, Engebretson M (2004) Appearance of quasi-monochromatic Pc34 pulsations in the polar cap. Geomagn Aeron 44:42–48

Chugunova OM, Pilipenko VF, Engebretson M, Rodger AS (2006) Statistical characteristics of the spatial distribution of Pc3-4 geomagnetic pulsations at high latitudes in the antarctic regions. Geomagn Aeron 46:64–73, doi:10.1134/S0016793206010075

De Lauretis M, Francia P, Vellante M, Piancatelli A, Villante U, Di Memmo D (2005) ULF geomagnetic pulsations in the southern polar cap: simultaneous measurements near the cusp and the geomagnetic pole. J Geophys Res 110:A11204, doi:1029/2005JA011058

De Lauretis M, Francia P, Regi M, Villante U, Piancatelli A (2010) Pc3 pulsations in the polar cap and at low latitude. J Geophys Res 115:A11223, doi:10.1029/2010JA015967

Eastwood JP, Balogh A, Dunlop MW, Horbury TS, Dandouras I (2002) Cluster observations of fast magnetosonic waves in the terrestrial foreshock. Geophys Res Lett 29:2046–2049

Eastwood JP, Balogh A, Lucek EA (2003) On the existence of Alfven waves in the terrestrial foreshock. Ann Geophys 21:1457–1465

Engebretson MJ, Posch JL, Pilipenko VA, Chugunova OM (2006) ULF waves at very high latitudes. In: Takahashi K, Chi PJ, Denton RE, Lysak RL (eds) Magnetospheric ULF waves: synthesis and new directions. Geophys. Monogr. Ser, vol 169. AGU, Washington, D.C, pp 137–156, doi:10.1029/169GM10

Francia P, De Lauretis M, Vellante M, Villante U, Piancatelli A (2009) ULF geomagnetic pulsations at different latitudes in Antarctica. Ann Geophys 27:3621–3629

Francia P, Regi M, De Lauretis M, Villante U, PV A (2012) A case study of upstream wave transmission to the ground at polar and low latitudes. J Geophys Res 117:A01210, doi:10:1029/2011JA016751

Francia P, Regi M, De Lauretis M (2013) ULF fluctuations observed along the SEGMA array during very low solar wind density conditions. Planet Space Sci 81:74–81

Glassmeier K-H, Motschmann U, Dunlop M, Balogh A, Acuna MH, Carr C, Musmann G, Fornacon K-H, Schweda K, Vogt J, Georgescu E, Buchert S (2001) Cluster as a wave telescope – first results from the fluxgate magnetometer. Ann Geophys 19:1439–1447

Hoppe MM, Russell CT (1983) Plasma rest frame frequencies and polarizations of the low-frequency upstream waves - ISEE 1 and 2 observations. J Geophys Res 88:2021–2027

Howard TA, Menk F (2005) Ground observations of high latitude Pc3-4 ULF waves. J Geophys Res 110:A04205, doi:10.1029/2004JA010417

Kobel E, Flückiger EO (1994) A model of the steady state magnetic field in the magnetosheath. J Geophys Res 99(A12):23617–23622, doi:10.1029/94JA01778

Krauss-Varban D, Omidi N (1991) Structure of medium Mach number quasi-parallel shocks: upstream and downstream waves. J Geophys Res 96:17715–17731

Le G, Russell CT (1992) A study of ULF wave foreshock morphology – II spatial variation of ULF waves. Planet Space Sci 40:1215–1225

Menk FW, Waters CL, Fraser BJ (2000) Field line resonances and wave guide modes at low latitude: 1. Observations. J Geophys Res 105:7747–7762

Narita Y, Glassmeier K-H, Schäfer S, Motschmann U, Fränz M, Dandouras I, Fornaçon K-H, Georgescu E, Korth A, Rème H, Richter I (2004) Alfven waves in the foreshock propagating upstream in the plasma rest frame: statistics from Cluster observations. Ann Geophys 22:2315–2323

Peredo M, Slavin JA, Mazur E, Curtis SA (1995) Three-dimensional position and shape of the bow shock and their variation with Alfvenic, sonic and magnetosonic Mach numbers and interplanetary magnetic field orientation. J Geophys Res 100:7907–7916

Pilipenko VA, Mazur NG, Fedorov EN, Engebretson MJ (2008) Interaction of propagating magnetosonic and Alfven waves in a longitudinally inhomogeneous plasma. J Geophys Res 113:A08218, doi:10.1029/2007JA012651

Regi M, Francia P, De Lauretis M, Glassmeier KH, Villante U (2013) Coherent transmission of upstream waves to polar latitudes through magnetotail lobes. J Geophys Res 118:1–9, doi:10.1002/2012JA018472

Regi M, De Lauretis M, Francia P (2014) The occurrence of upstream waves in relation with the solar wind parameters: a statistical approach to estimate the size of the foreshock region. Planet Space Sci 90:100–105

Rème H, Aoustin C, Bosqued JM, Dandouras I, Lavraud B, Sauvaud JA, Barthe A, Bouyssou J, Camus T, Coeur-Joly O, Cros A, Cuvilo J, Ducay F, Garbarowitz Y, Medale JL, Penou E, Perrier H, Romefort D, Rouzaud J, Vallat C, Alcaydé D, Jacquey C, Mazelle C, d'Uston C, Möbius E, Kistler LM, Crocker K, Granoff M, Mouikis C, Popecki M et al (2001) First multispacecraft ion measurements in and near the Earth's magnetosphere with the identical Cluster ion spectrometry (CIS) experiment. Ann Geophys 19:1303–1354, doi:10.5194/angeo-19-1303-2001

Russell CT, Childers DD, Coleman PJ Jr (1971) OGO 5 observations of upstream waves in interplanetary medium: discrete wave packets. J Geophys Res 76:845–861

Russell CT, Luhmann JG, Odera TJ, Stuart WF (1983) The rate of occurrence of dayside Pc3,4 pulsations - the L-value dependence of the IMF cone angle effect. Geophys Res Lett 10:663–666, doi:10.1029/GL010i008p00663

Shevyrev NN, Zastenker GN, Eiges PE, Richardson JD (2006) Low frequency waves observed by Interball-1 in foreshock and magnetosheath. Adv Space Res 37:1516–1521

Shue J-H, Chao JK, Fu HC, Russell CT, Song P, Khurana KK, Singer HJ (1997) A new functional form to study the solar wind control of the magnetopause size and shape. J Geophys Res 102:9497

Takahashi K, McPherron RL, Teresawa T (1984) Dependence of the spectrum of Pc3-4 pulsations on the interplanetary magnetic field. J Geophys Res 89:2770–2780

Vellante M, Villante U, De Lauretis M (1989) An analysis of micropulsation events at a low-latitude station during 1985. Planet Space Sci 37:767–773

Vellante M, Förster M, Pezzopane M, McKinnell LA, Jakowski N (2009) Remote sensing of the plasmasphere mass density by geomagnetic field line resonances detected at SEGMA array during the last solar cycle. 11th IAGA Scientific Assembly, Sopron, Hungary, 23–30 Aug 2009

Yumoto KA (1985) Low-frequency upstream wave as a probable source of low-latitude Pc 3–4 magnetic pulsations. Planet Space Sci 33:239–249

doi:10.1186/1880-5981-66-43
Cite this article as: Regi *et al.*: The propagation of ULF waves from the Earth's foreshock region to ground: the case study of 15 February 2009. *Earth, Planets and Space* 2014 **66**:43.